https://doi.org/10.1016/j.ijmultiphaseflow.2017.07.002

Dynamics of droplet impact on solid surface with different roughness

Chenglong Tang[a], Mengxiao Qin[a], Xinyan Weng[a], Xuhui Zhang[a], Peng Zhang[b], Jianlin Li[c],and Zuohua Huang[a]

[a] *State Key Laboratory of Multiphase Flow in Power Engineering, Xi'an Jiaotong University, Xi'an, 710049, China*

[b] *Department of Mechanical Engineering, the Hong Kong Polytechnic University, Kowloon, Hong Kong*

[c] *School of Power & Energy, Northwest Polytech University, Xi'an, 710072, China*

Abstract: This paper reports an experimental investigation on the impact dynamics of droplets (water, decane, ethanol, and tetradecane) onto a flat stainless steel surface, using high-speed microphotography and with a particular interest in the effect of surface roughness on the impact dynamics. Results show that the impacting water droplet spreads on the surface in the form of a rim-bounded lamella and the rim contracts back after reaching the maximum spreading, while this contraction motion is absent for the fuel liquids. With the increase of Weber number (*We*) and surface roughness, splashing, evidenced by the ejection of secondary droplets, is favored. The droplet spreading, which is characterized by a normalized diameter β, is accelerated with increasing *We*, while the surface roughness and Ohnesorge number (*Oh*) tend to slow down the spreading process. Furthermore, the maximum normalized spreading diameter, β_{max}, depends primarily on the (*We*/*Oh*) and the increase in the surface roughness slightly reduces β_{max}. The transition from spreading to splashing is enhanced with increasing *We* or R_a or both. An empirical correlation of β_{max} as a function of the surface roughness was derived based on the present experimental data. In addition, the transition from spreading to splashing can be represented by a critical $(We/Oh)^{1/2}$, which was fitted as a function of the surface roughness. All the proposed empirical correlations show good agreement with literature data and are believed to be of importance for the spray/wall interaction modelling.

Keywords: Droplet impact; surface roughness; spreading diameter; transition from spreading to

splashing

* Corresponding author;

Chenglong Tang, Associate Professor,

State Key Laboratory of Multiphase Flows in Power Engineering,

Xi'an Jiaotong University, Xi'an, 710049, People's Republic of China

Phone: 86-29-8266-5075, Fax: 86-29-8266-8789

Email: chenglongtang@mail.xjtu.edu.cn

1. Introduction

Spray impingement onto solid walls occurs in a variety of liquid-fueled engines. For instance, high-speed diesel engines and gasoline direct injection (GDI) engines have more compact combustors, so the spray would frequently impact the chamber walls due to the limited space for its development. For port fuel injection gasoline engines, a significant amount of fuel impinges the wall of the port or the back of the intake valves. With the increasing interest in engine downsizing, understanding the phenomena of spray impingement and the component droplet impingement has become correspondingly urgent. There are several practical issues related to droplet impingement in engines as follows. First, if the deposited liquid fuel is not totally evaporated and hence burned, it will reduce the total combustion efficiency and contribute to the emission of unburned hydrocarbon, especially under engine warm-up stage (Matsui and Sugihara, 1987). Second, droplet impact may result in splash, which influences the near wall mixture formation process. The splashed fuel and its vapor within the flame quenching layer would not be burned due to wall quenching, and consequently again contributes to the emission of unburned hydrocarbon (Chou and Patterson, 1995); Third, in supercharged GDI engine, gas-phase "hot spot" can be formed near the chamber wall due to fuel evaporation, which has been suggested to be the cause of the recently observed catastrophic event of super knock (Kalghatgi and Bradley, 2012); Finally, modelling spray impingement depends on the fidelity of the embedded sub-models of droplet impact (Bai and Gosman, 1995). In addition to the relevance of droplet impact in the above combustion engine applications, the fundamental impact dynamics of droplets are also important in the scenario of inkjet printing in microelectronics (Lim et al., 2009), spray coating (Bergeron et al., 2000; Sampath and Herman, 1996), spray cooling (Jia and Qiu, 2003; Kim, 2007; Pasandideh-Fard et al., 2001), and even prevention of the blade erosion in gas turbines (Mann and Arya, 2003; Tobin et al., 2015).

The droplet impact dynamics depends on the parameters of the droplet, the surface and the local gas layer near the wall. The droplet is characterized by its diameter D_0, velocity U_0 and impaction angle, density ρ, viscosity μ, and surface tension σ. The surface condition is characterized by its wettability (i.e. hydrophilic or hydrophobic), material, dry/wet (i.e. with/without liquid film), roughness R_a, and temperature T_w. The ambient gas pressure and hence density was also found to

play an important role in determining the impact outcomes (Stevens, 2014; Xu et al., 2005b). In order to quantify the impact outcomes, previous studies have adopted several important non-dimensional parameters, with the most important ones being the Weber number $We = \rho D_0 U_0^2/\sigma$, Ohnesorge number $Oh = \mu/\sqrt{\rho\sigma D_0}$, and Reynolds number $Re = \sqrt{We}/Oh$.

Focusing our interest on droplet impact on dry surfaces, we first note that only the hydrodynamic aspects of the impact need to be considered if the surface is unheated. Specifically, the droplet will deposit on the surface if the impact energy is relatively small. Upon contacting the surface, the droplet forms a lamella, which is bounded by a thicker rim and spreads out until a maximum radius, D_{max}, is reached. Whether the lamella contracts back depends on the competition among the surface tension force, the inertia, and the liquid viscous force. Several empirical and theoretical models for the evaluation of D_{max} have been proposed (Clanet et al., 2004; Roisman et al., 2002; Tran et al., 2012), showing that the non-dimensional maximum spreading diameter, $\beta_{max}= D_{max}/D_0$, lies in the range between 1 to 5. We note that the maximum spreading diameter is pertinent in the absence of splash and it could be different in high Weber number splashing cases. When the impact energy is sufficiently large, the droplet disintegrates and splashes into a number of secondary droplets. Regardless of the splashing, the spreading diameter of the primary droplet can still be used to describe the dynamics of the spreading process. There are extensive studies (Bayer and Megaridis, 2006; Clanet et al., 2004; Eggers et al., 2010; Laan et al., 2014; PasandidehFard et al., 1996; Roisman et al., 2002; Scheller and Bousfield, 1995; Sen et al., 2014; Seo et al., 2015; Ukiwe and Kwok, 2005) on β_{max} and several empirical or theoretical models have been developed to correlate β_{max} with non-dimensional parameters. However, the effect of surface roughness has been barely considered.

For the spray/wall interaction modeling, identifying different outcomes of a single droplet impact and developing the corresponding transition criterion are important because they determine the post-impact mass, momentum and energy distributions of the droplets. It has been shown that there are different types of splash impaction: corona, prompt and fingering splashes. Corona splash occurs on a smooth surface where the outer rim of the expanding lamella is lifted off the surface to form a corona shaped structure, from which a number of secondary droplets are subsequently ejected.

Xu et al. (2005) showed that corona splash can be suppressed by reducing the ambient pressure. Prompt splash occurs on a rough surface as secondary droplets are created at the spreading contact line immediately after impact. Fingering splash is suggested to be caused by the Rayleigh-Taylor instability at the rim of the expanding lamella (Allen, 1975). Thoroddsen and Sakakibara (1998) showed that the fingers can also split and merge during spreading due to the presence of the air trapped under the droplet. Various attempts have been made to identify the criteria for the splashing threshold.

Only a few studies have considered the effects of the surface roughness. Specifically, Stow and Hadfield (1981) and Mundo et al. (1995) used the parameter $K = We \cdot Re^{1/2}$ as a function of surface roughness to characterize the impaction outcomes. A critical K_c, above which the impaction results in splash, was obtained by fitting their experimental data. However, their experimental images are not sufficiently resolved to distinguish if the splash is corona, prompt, or fingering. Range and Feuillebois's criterion (1998) for splash threshold was based on the critical Weber number, which depends on the surface roughness. Cossali et al. (1997) have proposed an empirical model based on the data reported in (Mundo et al., 1995; Stow and Hadfield, 1981). Latka et al. (2012), and Xu et al. (2005) showed that thin-sheet splash (corona splash) is only observed for very smooth surface. Increasing roughness inhibits thin-sheet splash and promotes the prompt splash. Roisman et al. (Roisman et al., 2015) found that on rough substrates the main parameters that induce splash are the impact Weber number and the characteristic slope of the roughness of the substrate. They have proposed an empirical correlation for the prompt splash on rough and porous substrates based on their experimental data. Various criteria for splash threshold were reviewed by Moreira et al. (2010), and Josserand and Thoroddsen (2016), who pointed out that the discrepancies of the splash threshold criteria are due to the fuzzy identification of splash, the inadequate understanding of the complex flow and the difficulties to accurately describe the boundary conditions.

Besides the effect of surface roughness on those splashing threshold, extensive studies have demonstrated the influence of surface groove-texture geometry on the wetting behavior. When a droplet impacts on a rough surface, the actual wetting behavior can reside in the Cassie, Wenzel, or the intermediate state. The Cassie state (Cassie and Baxter, 1944) describes the situation when the

droplet contacts only with the peaks of the rough surface and there are “gas pockets” between these peaks under the droplet. The Wenzel state (Wenzel, 1936) is that the droplet is impregnated into the valleys and fully contacts with the rough surface. Recent experimental and theoretical works by Vaikuntanathan and Sivakumar (Vaikuntanathan and Sivakumar, 2014; Vaikuntanathan and Sivakumar, 2016) on droplet impact on groove-textured surfaces have emphasized the influence of the impact inertia, and the amplitude and geometry of the surface roughness. However, a quantitative dependence of the transition criterion on the surface roughness is still to be obtained, as advocated in the recent reviews by Yarin (2006), and Josserand and Thoroddsen (2016).

The objectives of this work are in the following. From an engineering point of view, inner walls of the engines such as the piston head, cylinder head and cylinder wall are produced with different surface treatment techniques with varying surface roughness. Previous spray impingement models do lack the implementation of the fundamental knowledge of the droplet impact dynamics, especially for surfaces with varying roughness. In addition, the surface roughness induces change of the wetting behavior at the length scales of surface roughness but its effects on the droplet spreading dynamics and energy balance still remain unknown. Thus we firstly aim to investigate the effect of surface roughness on the droplet spreading phenomenon by using enhanced high-speed imaging with high spatial and temporal resolutions. The droplet spreading diameter evolution, and the maximum spreading diameter can be therefore quantified with accuracy. Additionally, the limitation of previous studies by the inadequate imaging capabilities behooves us to precisely identify the transition boundaries of different impact outcomes with particular interests in quantifying the effects of the liquid properties and surface roughness. Finally, based on the experimental measurements, practically useful formulas for predicting the spreading diameter, and transition boundary between splashing and spreading will be proposed, in hopes that they can help advance the spray/wall interaction modeling for the computer simulations of I.C. engines.

2. Experimental specifications

2.1. System specification

The experimental system is sketched in Figure 1, which consists of the droplet generation

system, the high-speed imaging system, and the solid surface with temperature control. Droplets are generated at the tip of a hypodermic needle mounted on a three-dimensional positioner and falls vertically onto the horizontal, dry, stainless steel surface. The droplet impact process was recorded by a Phantom V611 high speed camera, attached by a long focus microscope and operated at 10,000 fps. The droplet release height H is adjustable and the velocity before impact can be obtained from analyzing the high-speed images. The experiments were conducted at room temperature (20ºC) and atmospheric pressure.

2.2. Characterization of droplet and solid surface

Figure 2(a) presents typical droplet information of about 30 dropping experiments. The high-speed camera with the long focus microscope has a target window of the resolution of 1104×504 and the window view was first calibrated by a standard micro-ruler with an accuracy of 0.01 mm. The size of an impacting droplet was measured by analyzing the images captured by the high-speed video camera Phantom V611. The impact velocity was obtained from two successive frames, in which the droplet moves around 200 pixels. The measured droplet velocity, U_0 , as a function of the release height, H, is shown in Figure 2(b) and it agrees well with the prediction of Ref. (Range and Feuillebois, 1998) by using the equation $U_0 = \sqrt{\frac{g}{A}(1-\exp(2A(D_0-H)))}$, $A = \frac{3}{4}\frac{\rho_{air} C_f}{\rho D_0}$, where g is the gravitational acceleration, D_0 is the diameter of the droplet, C_f is the friction coefficient, and ρ_{air} is the density of air. Note that to capture part of the horizontal surface morphology, we have tilted camera by 15^0, thus the vertical velocity obtained from high speed image is corrected with the cosine value of 15 degrees. The free fall speed over-predicts the impact velocity for larger falling heights. The estimated maximum error in the droplet shape is about 2 pixels (equivalent to 0.02mm with a 0.01mm/pixel spatial resolution). Consequently, the uncertainty of D_0 is about ± 0.04 mm, and that of U_0 is less than 2%. As a result, the relative error of the Weber number, $\Delta We/We = \Delta D_0/D_0 + 2\Delta U/U$, is less than 6%. The droplet sphericity can be quantified by S=min(D_{0H}/D_{0V}, D_{0V}/D_{0H}) , where D_{0H} and D_{0V} are the droplet size measured in the horizontal and vertical direction, respectively. For a typical ethanol droplet shown in Figure 2(a), the diameter is 1.9 ± 0.03 mm, and S is 1.0±0.05, indicating that the droplet sphericity is satisfactory and repeatable. The similar repeatability was observed for

other liquids.

Five standard reference specimens with elevated mean roughness (R_a = 0.025 ~ 6.3 μm) were used as the target surfaces. Figure 3 shows the relative roughness intensity as a function of the measuring location for different solid surfaces. These surface roughness data were measured by using a surface roughometer (Trimos TR Profile VH 6001). It is seen that R_a well represents the surface roughness of the standard reference specimens.

The liquids used in this work include deionized water, ethanol, decane, and tetradecane. The physical properties of these liquids are presented in Table 1. Surface tension of water is approximately 3 times larger than those of the other liquids while tetradecane has a higher viscosity than the other liquids.

3. Phenomenological Descriptions

3.1 On smooth surface (R_a =0.025μm)

Figure 4 presents typical images of a water droplet impacting on a smooth surface (R_a=0.025μm), with varying Weber numbers. Five typical instants for each impacting case were selected for demonstration. Detailed process of each impacting is shown in the Supplemental Videos **1-3** (all impact cases listed are supplemented with their videos). At t = 0 ms, the dash-dot line denotes the impacting plane. The impacting droplet is above the line and the droplet inverted inflection on the plane is under the line. Case 1 shows the low *We* impact (*We* = 25) on smooth surface. Upon impact, the bottom of the droplet forms a thin layer, above which the droplet deforms to resemble a truncated sphere, as shown at t = 0.4 ms. Subsequently, the bottom liquid of the droplet spreads out radially to form a lamella (bounded by a thick and smooth rim), which reaches the maximum spreading diameter D_{max} at t = 4.1 ms. After then (see Video 1 after t = 4.1 ms) the rim liquid contracts back and the rim grows thicker and thicker until its inner boundary (defined in Figure 4) merges and an upward jet is formed, which subsequently damped through several periods of oscillation and the liquid attains a final equilibrium spreading diameter D_{eq} smaller than D_{max}. The initial kinetic energy of droplet is partly dissipated by oscillation and partly converted into the increased surface energy. We note that the outer periphery of the rim represents the contact line, thus

for water droplet impact, the contact line advances in the spreading phase and recedes in the contracting and relaxation phase.

As *We* increases (*We* = 193), D_{max} increases and the spreading is faster due to the larger impact inertia (case **2** and Supplemental Video 2), although the impact still results in spreading followed by contraction. The difference is that the rim is thinner than that of case 1 and there is some small "finger-like" disturbance around the rim. When *We* is further increased as shown in case **3** (*We* =971), the disturbance of the thinner rim is more prominent. However, no secondary droplets are observed for all the Weber numbers studied here.

Figure 5 presents typical images of a decane droplet impacting on a smooth surface (R_a=0.025μm). The different observations from those for water can be made as follows. First, for the high *We* case (*We*= 546, case **6**), splashing is observed as very fine secondary droplets are ejected from the rim immediately after impact. We can clearly see those secondary droplets in the inset figure (more obviously shown in Supplemental Video **6**). Second, for all the Weber numbers, decane droplet (and other liquids such as ethanol and tetradecane) does not contract back after the droplet spreading reaching the D_{max} and there is no receding contact line motion. Finally, "finger-like" disturbance around the rim is much less prominent than that for water, even at high Weber number (case **6**). We note for this kind of splash, the secondary droplets are immediately ejected from the spreading contact line and thus it is defined as prompt splash (Xu, 2007). In addition, the corona splash that were typically observed by (Xu, 2007; Xu et al., 2005a) for very smooth surface, and by (Latka et al., 2012) for very viscous liquids were not observed in this work.

Figure 6 shows images of the different liquid droplet impacting on a smooth surface (R_a =0.025μm) at We ≈ 20. The images show that the droplet spreading for decane (case **4**), ethanol (case **7**), and tetradecane (case **8**) are very similar but different from case **1** for water. Upon impact, the bottom of the truncated spherical droplet spreads out radially to form a lamella (bounded by a thick and smooth rim), reaching a maximum spreading diameter D_{max}. Then the outer edge of the rim is locked and the inner edge of the rim keeps on contracting, and finally merges. For high Weber number impact shown in Figure 7 (*We* ≈100, cases **9**-**12**), the impact outcome is still spreading, which is faster and D_{max} is increased due to the increased inertia. For *We*≈ 300, as shown in Figure 8, splashing outcome

is observed for tetradecane (case **15**), while for decane (case **13**) and ethanol (case **14**), still no secondary droplets are seen after impact.

3.2 On rough surfaces (R_a =0.1-6.3 μm)

Figure 9 presents the images of a water droplet impacting on solid surfaces with increased R_a at We ≈ 200. With the increase of R_a, as shown by case **16**, **17**, and **18**, the impacting outcome is spreading, and the "finger-like" disturbance around the rim becomes increasingly obvious. When R_a is increased to 6.3 μm, as shown in case **19**, the outer edge of the rim disturbance is lifted-up immediately after the droplet impact (t = 0.4 ms). The droplet keeps spreading and the "finger fluid" keeps accumulating until the spreading reaches D_{max}. Subsequently, the rim tends to contract back while the "finger fluid" is not able to be pulled back due to its inertia and is pinched off from the outer rim, resulting in secondary droplets, as shown by the marked circle.

Figure 10 shows the effect of surface roughness for tetradecane droplet impact with $We \approx 250$. For relatively smooth surface (case **20**), the "finger-like" disturbance grows immediately upon impact, as shown by the image at t = 0.4 ms. These disturbance is subsequently smoothed as the lamella spreads out and the disturbance is then merged with the outer rim. The "finger fluid" does not have enough inertia to breakup from the lamella. For the same R_a with higher impact inertia, as shown by case **15** in Figure 8, the "finger" fluid pinches off the lamella and results in splash because the "finger" fluid has enough inertia to break itself from the decelerating lamella. With the increase of R_a, as shown by cases **21**, some small secondary droplets are ejected at the periphery of the rim and the impact outcome is splash, as shown by image at t = 1.0 ms. With the increase of R_a, shown by cases **22-24**, the splash becomes increasingly prominent, indicating that surface roughness promotes splashing.

4. Droplet spreading dynamics

To quantify the droplet impact dynamics, the normalized droplet spreading diameter $\beta = D/D_0$ as a function of normalized time $\tau = tU_0/D_0$ for all test cases are presented. We note that β measures the normalized spreading diameter of the wetted spot on the solid surface and that the evolution of β

actually represents the motion of the contact line if the impact outcome is spreading. When the impact outcome is splashing with some secondary droplets ejected from the periphery of the contact line, the normalized spreading diameter is still instructive for the dynamics of the residual fluid. However, under the scenario of droplet splashing, $\beta_{max\text{-}res}$ (maximum normalized spreading diameter of the residual fluid) should be used to represent the maximum diameter of the contact area.

4.1 Different spreading stages on a smooth surface

For droplet impact on a relatively smooth surface (R_a =0.025 μm), Figure 11a shows the normalized droplet spreading diameter evolution for decane. Different stages of spreading, such as *kinematic*, *spreading*, *relaxation* and *equilibrium* , can be identified. Specifically for *We* = 18, in the initial kinematic stage ($\tau < 0.1$) during which no spreading lamella has yet formed, β is smaller than 1 and it increases with τ according to a power law with an exponent of around 0.5.We note that for all the impacting parameters (*We* and *Oh*) and solid surfaces (R_a) studied here, the evolution of β in this stage follows this power law and the uncertainty comes from the limited data points because at high Weber number impact condition, only a few images can be collected before β grows to 1. This observation is consistent with that reported by Rioboo et al. (2002) where the exponent lies between 0.45 and 0.57. In the subsequent spreading stage, a lamella is formed from the bottom of the droplet and is bounded by a thicker rim and β grows larger than 1. At $\tau \approx$ 2.8, β grows to β_{max} and the contact line is fixed at D_{max}.-Mechanistically, the spreading dynamics is controlled by the spreading inertia which is progressively weakened by the retarding viscous and surface tension forces as time proceeds. This is substantiated by the gradually decreasing slope of the β-τ curve after the kinematic phase, corresponding to slowed down contact line velocity.

With the increase of Weber number (*We* = 97 and 195), the evolution of β becomes steeper, indicating a faster spreading and higher contact line velocity. In addition, β_{max} increases with *We* while it takes longer normalized time to reach β_{max}, because the spreading is inertia driven, and larger *We* means larger droplet inertia. We note that *t* in millisecond for reaching β_{max} is actually decreased with the increase of Weber number (t_{max} = 103, 74, and 56 ms, respectively for *W*e = 18, 97, and 195) because of faster spreading. Further increase in Weber number (*W*e = 395) results in splashing outcome and secondary droplets are ejected upon impact (Figure 5, case **6**). We nevertheless still plot

the normalized spreading diameter of the residual fluid. It is seen that the spreading of the residual lamella is still faster than the case of *We* = 195 though some mass has been ejected.

For water droplet impact cases as shown in Figure 11b, the outcome is all spreading at R_a=0.025 μm in the present Weber number range. The spreading process can be also divided into different stages, namely, *kinematic*, *spreading*, *receding* and *equilibrium*. The increase in Weber number leads to faster spreading, larger β_{max}, and longer time to reach β_{max}, which is similar to that for decane. This is expected because with the increase of Weber number, the kinetic energy upon impact is increased, which needs to be balanced by larger surface surface energy of the spreading surface and higher viscouse dissipation before the liquids stays equilibrium. After reaching β_{max}, however, the contact line contracts back because of the capillary force, and this contact line motion is different from that for decane, ethanol, or tetradecane.

The normalized spreading diameter evolution for different liquids are compared at different Weber numbers as shown in Figure 12. We note that for sufficiently high Weber numbers, there will be splashing for ethanol and tetradecane, as shown in Fig. 12(d). It is seen that for all the Weber number cases (no matter the impact outcome is splashing or spreading), decane, ethanol and tetradecane droplet impacts do not show receding behavior after reaching β_{max}, while water droplet impacts lead to decrease in β after it reaches β_{max}, as discussed in the preceding section. In addition, the decane droplet impact yields slightly faster spreading, ethanol the second, and tetradecane the slowest. Since decane, ethanol and tetradecane have close surface tension while the viscosity increases sequentially, and the Reynolds number actually decreases for *We*~20 impact (858, 725, and 394, respectively for decane, ethanol and tetradecane), there is a increasingly profound influence of viscous dissipation for decane, ethanol, and tetradecane. Consequently, the spreading is slower in the order decane, ethanol, and tetradecane. In addition, the β_{max} (for spreading outcome) and $\beta_{max\text{-}res}$ (for splashing outcome) also decrease in this liquid property order. However, the normalized time to reach β_{max} or $\beta_{max\text{-}res}$ seems not to be affected by different liquids, as long as their Weber number is fixed, confirming the dominant influence of Weber number on $\tau_{max,}$ as shown in Figure 11.

Comparing the evolution of β evolution for decane and water droplet impact, we can see that two curves almost overlap before reaching β_{max}. However, β_{max} for water is smaller than decane at

relatively smaller Weber number (Figure 12a). With the increase of Weber number, the difference in β_{max} between decane and water droplet impact gradually vanishes. This is because decane and water have close viscosity and hence similar viscous dissipation, while water have significantly higher surface tension, it needs smaller β_{max} to hold the same amount of surface energy than decane. Additionally, with the increase of Weber number, the difference in surface energy between decane and water at their β_{max} becomes less important compared with the increased initial kinetic energy and higher viscous dissipation.

4.2 Effects of surface roughness on the spreading dynamics: mass transfer, viscous loss

Figure 13 shows the effect of R_a on the β evolution for both tetradecane and water droplet impact. It is seen that for all the spreading outcome impact, the normalized spreading diameter for different R_a are almost the same for the stage when $\tau < 1.0$. Subsequently when R_a is increased, effect of R_a on β evolution and β_{max} is visible: larger R_a leads to slightly slower spreading and smaller β_{max}, as shown in Figure 13 (a) and (b). In addition, at higher Weber number, the effect of R_a seems to be less significant for the spreading case, as shown in Figure 13 (c) and (d). We note that at higher Weber number shown in Figure 13 (d) and (e), droplet impacts result in splashing outcome for surfaces with sufficiently high R_a. The normalized spreading diameter for splashing cases actually represents the residual liquid (after ejection of secondary droplets from the parent droplet) contact line motion. As a consequence, β for splashing outcome is slightly smaller than the spreading outcome impact (Figure 13 (d) for R_a = 6.3 μm cases) because of the lost mass, while they have parallel variation with respect to τ, compared with those spreading outcome impact cases at lower R_a.

We think that besides the enhanced trend of splashing, surface roughness amplitude R_a may induce other two mechanisms on β evolution on rough surfaces: mass transfer and viscous dissipation. Firstly, for small impact inertia at relatively small R_a, the surface roughness amplitude is small enough to enable direct contact and results in Wenzel state. As R_a increases, “gas-pocket” is trapped in a deeper valley and the wetting behavior is more like Cassie state. However, if the Weber number is large enough, the liquid can always be impregnated into the valleys of the rough surface and at this high inertia impact case, the increase in R_a just results in wetting an increased surface area. Recently, Vaikuntanathan and Sivakumar (Vaikuntanathan and Sivakumar, 2014; Vaikuntanathan and

Sivakumar, 2016) showed that the critical velocity, $U_{0,\text{Cas-Wenz}}$, beyond which the wetting state transitions from Cassie to Wenzel is lower than 0.9 ms^{-1} for their groove-textured surfaces, which is equivalent to the Weber number of around 30 for their droplet diameter of 2.6 mm. In addition, $U_{0,\text{Cas-Wenz}}$ decreases with the decrease in the intrinsic hydrophobicity and surface roughness amplitude. We note that in all cases studied here, the wetting behavior resides in the Wenzel state, because the minimum Weber number studied here is of the same order (O(10)) as the transition Weber number $We_{\text{Cas-Wenz}}$ studied Refs. (Vaikuntanathan and Sivakumar, 2014; Vaikuntanathan and Sivakumar, 2016), but the amplitude of surface roughness (54~300 μm) in Refs. (Vaikuntanathan and Sivakumar, 2014; Vaikuntanathan and Sivakumar, 2016) is much higher than R_a (0.025~ 6.3 μm) studied here in this work. In addition, their hydrophobicity effect is more profound than the cases studied in this work because their minimum static contact angle is around 76°, while our maximum static contact angle is 50° for water and around 5°, 7°, and 11° respectively for decane, ethanol and tetradecane. As a consequence, the present wetting behavior resides in the Wenzel state and the increase in R_a just results in wetting an increased surface area and trapping more liquids in the valleys of the rough surface. This contributes to the decelerated β evolution at higher R_a and this R_a effect is less influential at higher Weber numbers for the spreading outcome cases.

Secondly, Chamakos et al. (2016) numerically investigated the droplet spreading dynamics on a rough surface and previous limitations in the hydrodynamic model were overcome by implicit derivation of the friction forces at the contact line. We note that the normalized amplitude of surface roughness in Ref. (Chamakos et al., 2016) is 5.0 x 10^{-3}, which lies in the surface roughness levels studied in this work (2.5 x 10^{-5}~6.3 x 10^{-3} from R_a ~ 0.025 to 6.3 mm for droplet diameter D_0 of around 2 mm), which is smaller than the surface roughness amplitude of Refs. (Vaikuntanathan and Sivakumar, 2014; Vaikuntanathan and Sivakumar, 2016). In addition, the droplet impact velocity in Ref. (Chamakos et al., 2016) is larger than the Cassie to Wenzel transition velocity $U_{0,\text{Cas-Wenz}}$ (Vaikuntanathan and Sivakumar, 2014; Vaikuntanathan and Sivakumar, 2016), thus the wetting behavior simulated in Ref. (Chamakos et al., 2016) resides in the Wenzel state. Furthermore, Chamakos et al. (2016) showed that local viscous forces that become effective within the length scale of surface roughness amplitude leads to substantial energy loss at the contact line, resulting in

slightly decelerated contact line motion. This is also another mechanism that leads to decelerated contact line motion by increased R_a shown in Figure 13.

4.3 Empirical Correlation of β_{max}

The maximum spreading diameter has been previously reported for water droplet impact on solid surface and several empirical and theoretical models have been proposed (Bayer and Megaridis, 2006; Clanet et al., 2004; Eggers et al., 2010; Laan et al., 2014; PasandidehFard et al., 1996; Roisman et al., 2002; Scheller and Bousfield, 1995; Sen et al., 2014; Seo et al., 2015; Ukiwe and Kwok, 2005) and summarized in Table 2. It is seen that the effect of surface roughness on the β_{max} has not been considered. Some of these studies used smooth surface while the others did not specify the surface roughness, which behooves us to examine the surface roughness effect. In addition, we compared the previous models from Refs. (Scheller and Bousfield, 1995; Bayer and Megaridis, 2006 ; Laan et al., 2014; Roisman, 2009; Wildeman et al., 2016) with our experimental data in Figure 14. It's clear that on smooth surface, all the models show good prediction for water droplet impact. However, only the model of Wildeman et al. (2016) agrees well with the measurements for decane, tetradecane and ethanol droplets. In their review regarding the maximum spreading, Scheller and Bousfield (1995) stated that "the maximum spreading is independent of surface roughness", while our measurements shown in Figure 15 is not consistent with this statement. Specifically, our measurements show that for all the liquids studied here, a very fine power law dependence of $\beta_{max} \sim (We/Oh)^b$ ($b > 0$) was observed , indicating that the maximum spreading is favored at higher impact inertia (larger *We*) and for less viscous liquids (smaller *Oh*). The experimental data are fitted in to the power law by

$$\beta_{max} = a(We/Oh)^b \tag{1}$$

where the fitting constants are listed in Table 3.

For the smallest R_a studied here in this work, the exponent *b* for water droplet is around 0.26 and this is consistent with several empirical models (see Table 2).The exponent *b* for decane, ethanol and tetradecane droplets is around 0.15. In addition, with the increase of R_a, a moderate increase of *b* was observed, and the increase is stronger for water than for the other liquids. The experimentally

measured and the empirical model Eq.(1) predicted β_{max} for all the liquids and roughness are further compared in Figure 16 and the line represents the least square linear fitting. It shows that the empirical equation predicted versus the measured data for all the conditions lie on the line, and the fitting has a relative mean error of 0.03%, indicating that Eq.(1) describes well the β_{max} dependence on both *We*/*Oh* and the surface roughness for all the liquids studied in this work. Table 2 shows that there has been no literature data of β_{max} for well characterized rough surface. Previous published β_{max} data for smooth surface are then compared with our proposed empirical equation, as shown in Figure 17. The fitting parameters in Eq. (1) are the same for ethanol, decane and tetradecane (a=0.87, b=0.15), while for water, the fitting parameters are different (a=0.20, b=0.26), as shown in Table 3. Thus in Fig. 17(a), the comparison of the experimental data with Seo et al. (2015) and Sen et al. (2014) uses the fitting parameter of a=0.87 and b=0.15, while the comparison with Scheller and Bousfield (1995), Clanet et al. (2004), and Bayer and Megaridis (2006) for water uses the fitting parameters of a=0.20 and b=0.26, as in Fig. 17 (b). It is seen that Eq. (1) predictions agree well with all the previous measurements for smooth surface, with a relative mean error of 7.8%, and the difference comes from the slight variation of the surface roughness in Refs.(Bayer and Megaridis, 2006; Clanet et al., 2004; Scheller and Bousfield, 1995; Sen et al., 2014; Seo et al., 2015), indicating that Eq. (1) not only presents good prediction of β_{max} on rough surface, but also accommodates the smooth surfaces.

5. Transition criterion from spreading to splashing

The criterion for the transition from spreading to splashing is of significant importance for the spray/wall interaction modelling because it plays an important role in determining the post-impact droplets mass, momentum and energy distributions and will subsequently affect the near-wall mixture formation characterization.

5.1 Enhanced splashing on rough surfaces

Figure 18(a) and (b) show the measured critical Weber number, We_{cr}, for the transition from spreading to splashing, as a function of the normalized surface roughness. It is seen that R_a/D_0 has a

significant effect in promoting the splash, especially for droplets with smaller *Oh*. Specifically, for *Oh* = 0.002 water droplet impacting onto an R_a=0.025μm surface, the droplet would just spread over the surface without secondary droplets even for the largest *We* considered in this study (*We* = 971). For R_a = 0.1 μm and 6.3 μm, splashing was observed for sufficiently high Weber numbers, and the critical Weber number is respectively 379, and 155. Previous experiments and empirical models for spreading to splashing transition are summarized in Table 4. Stow and Hadfield (1981) proposed an empirical model in the form of $(D_0 U_0^{1.69})_{cr} \sim R_a$, and showed that the results for water droplet impacting stainless steel surface is similar to those of water/aluminium. Mundo et al. (1995) also proposed an empirical model in which $(OhRe^{1.25})_{cr}$ = 57.7 and in their model, the surface roughness effect is not included as they stated that "the surface roughness does not promote splashing". This seems to be contradictory with our measurements, however, the R_a and D_0 studied in Ref. (Mundo et al., 1995) is respectively in the range (2.8~78 μm) and (100~300 μm), so the normalized roughness $\ln(R_a/D_0)$ in Ref. (Mundo et al., 1995) is in the range between -4.7 and -0.2, and our measurements do show the flattened trend of We_{cr} at such large $\ln(R_a/D_0)$. Range and Feuillebois (1998) proposed an empirical model in the form of $We_{cr} = a_1 \log^{b_1}(R_a/D_0)$ and showed that the values of fitting constants a_1 and b_1 are different for different droplet-solid surface combinations. However, for ethanol droplets impacting stainless steel and aluminum surfaces, the fitting constants are similar and this similarity is consistent with the observation of Stow and Hadfield for water-stainless steel/aluminum combination. In addition, Cossali et al. (1997) fitted the experimental data of Mundo et al. (1995), and Stow and Hadfield (1981), and proposed the empirical criterion as $(WeOh^{-0.4})_{cr} = 649 + 3.76(R_a/D_0)^{-0.63}$. We have then re-organized previous empirical models of Stow and Hadfield (1981), Range and Feuillebois (1998), and Cossali et al. (1997) and compared with our measurements in Figure 18 (a). It is seen that the model of Stow and Hadfield (1981) shows moderately good agreement with the present measurements for water. However, the empirical model by Cossali et al. (1997) under-predicts the critical Weber number, though it was obtained by fitting the experimental data of Mundo et al. (1995) and Stow and Hadfield (1981).

5.2 Empirical correlation for spreading to splashing transition

In Sec 4.3, the non-dimensional parameter *We*/*Oh* was used as a variable for β_{max} correlation. This

parameter should be able to be used to distinguish different impact outcomes because it includes the factors that characterize the inertia, viscosity and surface tension effects. The inertia drives the movement of the contact line and higher inertia triggers the contact line instability, the viscous dissipation consumes certain amount of inertia and prohibits the splash and the surface tension tends to hold more surface potential and then inhibits the formation of secondary droplets. We then plotted the critical value of the transition value of $(We/Oh)^{1/2}$ as a function of the normalized roughness, and found they have a quasi-linear relationship as

$$K_{\mathrm{cr}} = (We/Oh)^{1/2}{}_{\mathrm{cr}} = c + d\ln(R_a/D_0) \tag{2}$$

where the fitting coefficients c and d , depending on different liquids, are shown in Table 3.

Figure 19 shows that Eq. (2) correlates all the present experimental measurements well. The slope of the linear fitting (i.e. d) is negative, indicating that the increase in surface roughness promotes splashing and therefore results in a smaller critical K_{cr}. In addition, with the decrease of Oh, the absolute slope value is increased, indicating that the surface roughness effect is more significant for less viscous liquids. Additionally, the fitting has a relative mean error of 0.16 %.

We have further compared our empirical correlation of Eq.(2) with available while limited experimental results data on the spreading to splashing threshold (Stow and Hadfield, 1981;Range and Feuillebois, 1998;Vander Wal et al., 2006a, b;Palacios et al., 2013). Because different experimental results used different forms of splashing threshold, these results are then reformulated to $(We/Oh)_{\mathrm{cr}}^{1/2}$as a function of $\ln(R_a/D_0)$, as shown in Figure 20. It is seen that the experimental data of Stow and Hadfield (1981) for water droplet/stainless steel surface showed excellent agreement with Eq.(2). The results from Vander Wal et al. (2006a, b) for ethanol, tetradecane, and decane droplet/relatively smooth aluminum surface and those from Palacios et al. (2013) for water and ethanol droplet/smooth glass surface also agree well with Eq. (2). The results for both water and ethanol droplet/aluminum surface from Range and Feuillebois (1998) also showed reasonably good agreement with the Eq.(2) prediction. However, their experimental results for water and ethanol droplet/glass surface overshoot the Eq.(2) prediction. The disagreement may originate from the surface material effect, not from the surface roughness effect. Generally, our proposed spreading to splashing criterion yields acceptable agreement with all the literature data.

6. Concluding remarks and future work

With the increasing interest in engine downsizing, spray wall interactions become more and more inevitable. Modeling the spray-wall impingement needs comprehensive understanding of the droplet impact dynamics under various roughness. In the present study, we have systematically investigated the dynamics of the droplet impact on cold and dry solid surfaces, emphasizing on the effect of surface roughness. High speed images show that although all the impacting liquid droplets spread on the surface in the form of a rim-bounded lamella, the water droplet contracts back after reaching the maximum spreading the fuel droplets do not have the contraction motion. To quantify the spreading behavior, the evolution of the non-dimensional droplet spreading diameter β becomes faster with increasing *We* while becomes slower with increasing the surface roughness and Ohnesorge number (*Oh*). Additionally, β_{max} depends primarily on (*We*/*Oh*) and is slightly reduced by the increase in the surface roughness. Empirical correlations of β_{max} as a function of the surface roughness were derived and show good agreement with both the present and previous experimental data. Increasing *We* and surface roughness, the impact outcome changes from spreading to splashing. The transition from spreading to splashing can be characterized by a critical value of $(We/Oh)^{1/2}$ and it was empirically fitted as a function of the surface roughness, which also shows reasonably good agreement with all the literature data. These empirical correlations are of significance for the spray/wall interaction modelling. One of the most important future work might be the droplet impact on wetted and/or heated solid surface which couples the complex effects of the hydrodynamics, heat transfer and phase change.

Acknowledgment

This work is supported by the National Natural Science Foundation of China (91541107, 51206131, and 51406158), the Science Challenge Project (JCKY2016212A501), and the Fundamental Research Funds for the Central Universities. The work at the Hong Kong Polytechnic University was supported by Hong Kong RGC/GRF (PolyU 152217/14E and PolyU 152651/16E).

References

Allen, R.F., 1975. Role of surface-tension in splashing. J. Colloid Interf. Sci. 51, 350-351.

Bai, C., Gosman, A.D., 1995. Development of methodology for spray impingement simulation. SAE paper No.950283

Bayer, I.S., Megaridis, C.M., 2006. Contact angle dynamics in droplets impacting on flat surfaces with different wetting characteristics. J. Fluid. Mech. 558, 415-449.

Bergeron, V., Bonn, D., Martin, J.Y., Vovelle, L., 2000. Controlling droplet deposition with polymer additives. Nature. 405, 772-775.

Cassie, A.B.D., Baxter, S., 1944. Wettability of porous surfaces. Trans. Faraday. Soc. 40, 0546-0550.

Chamakos, N.T., Kavousanakis, M.E., Boudouvis, A.G., Papathanasiou, A.G., 2016. Droplet spreading on rough surfaces: Tackling the contact line boundary condition. Phys. Fluids. 28, 022105.

Chou, T., Patterson, D.J., 1995. In-cylinder measurement of mixture maldistribution in a L-head engine. Comb. Flame. 101, 45-57.

Clanet, C., Beguin, C., Richard, D., Quere, D., 2004. Maximal deformation of an impacting drop. J. Fluid. Mech. 517, 199-208.

Cossali, G.E., Coghe, A., Marengo, M., 1997. The impact of a single drop on a wetted solid surface. Exp. Fluids. 22, 463-472.

Eggers, J., Fontelos, M.A., Josserand, C., Zaleski, S., 2010. Drop dynamics after impact on a solid wall: Theory and simulations. Phys. Fluids. 22, 062101.

Jia, W., Qiu, H.H., 2003. Experimental investigation of droplet dynamics and heat transfer in spray cooling. Exp. Therm. Fluid. Sci. 27, 829-838.

Josserand, C., Thoroddsen, S.T., 2016. Drop impact on a solid surface, Annu. Rev. Fluid. Mech. 365-391.

Kalghatgi, G.T., Bradley, D., 2012. Pre-ignition and 'super-knock' in turbo-charged spark-ignition engines. Int. J. Engine. Res. 13, 399-414.

Kim, J., 2007. Spray cooling heat transfer: The state of the art. Int. J. Heat Fluid. Fl. 28, 753-767.

Laan, N., de Bruin, K.G., Bartolo, D., Josserand, C., Bonn, D., 2014. Maximum diameter of impacting liquid droplets. Phys. Rev. Applied 2.

Latka, A., Strandburgpeshkin, A., Driscoll, M.M., Stevens, C.S., Nagel, S.R., 2012. Creation of prompt and thin-sheet splashing by varying surface roughness or increasing air pressure. Phys. Rev. Lett. 109, 1-6.

Lim, T., Han, S., Chung, J., Chung, J.T., Ko, S., Grigoropoulos, C.P., 2009. Experimental study on spreading and evaporation of inkjet printed pico-liter droplet on a heated substrate. Int. J. Heat Mass Tran. 52, 431-441.

Mann, B.S., Arya, V., 2003. HVOF coating and surface treatment for enhancing droplet erosion resistance of steam turbine blades. Wear 254, 652-667.

Matsui, Y., Sugihara, K., 1987. Sources of hydrocarbon emissions from a small direct injection diesel engine. SAE Paper No.871613

Moreira, A.L.N., Moita, A.S., Panão, M.R., 2010. Advances and challenges in explaining fuel spray impingement: How much of single droplet impact research is useful? Prog. Energ. Combust. 36, 554-580.

Mundo, C., Sommerfeld, M., Tropea, C., 1995. Droplet-wall collisions - experimental studies of the deformation and breakup process. Int. J. Multiphase Flow. 21, 151-173.

Palacios, J., Hernández, J., Gómez, P., Zanzi, C., López, J., 2013. Experimental study of splashing patterns and the splashing/deposition threshold in drop impacts onto dry smooth solid surfaces. Exp. Therm. Fluid. Sci. 44, 571-582.

Pasandideh-Fard, M., Aziz, S.D., Chandra, S., Mostaghimi, J., 2001. Cooling effectiveness of a water drop impinging on

a hot surface. Int. J. Heat Fluid. Fl. 22, 201-210.
PasandidehFard, M., Qiao, Y.M., Chandra, S., Mostaghimi, J., 1996. Capillary effects during droplet impact on a solid surface. Phys. Fluids. 8, 650-659.
Range, K., Feuillebois, F., 1998. Influence of surface roughness on liquid drop impact. J. Colloid Interf. Sci. 203, 16-30.
Rioboo, R., Marengo, M., Tropea, C., 2002. Time evolution of liquid drop impact onto solid, dry surfaces. Exp. Fluids. 33, 112-124.
Roisman, I.V., 2009. Inertia dominated drop collisions. II. An analytical solution of the Navier–Stokes equations for a spreading viscous film. Phys. Fluids. 21, 052104.
Roisman, I.V., Lembach, A., Tropea, C., 2015. Drop splashing induced by target roughness and porosity: The size plays no role. Adva. Colloid Interf. Sci. 222, 615-621.
Roisman, I.V., Rioboo, R., Tropea, C., 2002. Normal impact of a liquid drop on a dry surface: Model for spreading and receding. P. Roy. Soc. Lond. A Mat. 458, 1411-1430.
Sampath, S., Herman, H., 1996. Rapid solidification and microstructure development during plasma spray deposition. J. Therm. Spray. Technol. 5, 445-456.
Scheller, B.L., Bousfield, D.W., 1995. Newtonian drop impact with a solid-surface. Aiche J. 41, 1357-1367.
Sen, S., Vaikuntanathan, V., Sivakumar, D., 2014. Experimental investigation of biofuel drop impact on stainless steel surface. Exp. Therm. Fluid. Sci. 54, 38-46.
Seo, J., Lee, J.S., Kim, H.Y., Yoon, S.S., 2015. Empirical model for the maximum spreading diameter of low-viscosity droplets on a dry wall. Exp. Therm. Fluid. Sci. 61, 121-129.
Stevens, C.S., 2014. Scaling of the splash threshold for low-viscosity fluids. EPL. 106, 24001.
Stow, C.D., Hadfield, M.G., 1981. An experimental investigation of fluid-flow resulting from the impact of a water drop with an unyielding dry surface. P. Roy. Soc. Lond. A Mat. 373, 419-441.
Thoroddsen, S.T., Sakakibara, J., 1998. Evolution of the fingering pattern of an impacting drop. Phys. Fluids. 10, 1359-1374.
Tobin, E.F., Rohr, O., Raps, D., Willemse, W., Norman, P., Young, T.M., 2015. Surface topography parameters as a correlation factor for liquid droplet erosion test facilities. Wear. 328, 318-328.
Tran, T., Staat, H.J.J., Prosperetti, A., Sun, C., Lohse, D., 2012. Drop impact on superheated surfaces. Phys. Rev. Lett. 108, 036101.
Ukiwe, C., Kwok, D.Y., 2005. On the maximum spreading diameter of impacting droplets on well-prepared solid surfaces. Langmuir. 21, 666-673.
Vaikuntanathan, V., Sivakumar, D., 2014. Transition from Cassie to impaled state during drop impact on groove-textured solid surfaces. Soft Matter. 10, 2991-3002.
Vaikuntanathan, V., Sivakumar, D., 2016. Maximum spreading of liquid drops impacting on groove-textured surfaces: effect of surface texture. Langmuir. 32, 2399-2409.
Vander Wal, R.L., Berger, G.M., Mozes, S.D., 2006a. The combined influence of a rough surface and thin fluid film upon the splashing threshold and splash dynamics of a droplet impacting onto them. Exp. Fluids. 40, 23-32.
Vander Wal, R.L., Berger, G.M., Mozes, S.D., 2006b. The splash/non-splash boundary upon a dry surface and thin fluid film. Exp. Fluids. 40, 53-59.
Wenzel, R.N., 1936. Resistance of solid surfaces to wetting by water. Ind. Eng. Chem. 28, 988-994.
Wildeman, S., Visser, C.W., Sun, C., Lohse, D., 2016. On the spreading of impacting drops. J. Fluid. Mech. 805, 636-655.
Xu, L., 2007. Liquid drop splashing on smooth, rough, and textured surfaces. Phys. Rev. E. 75, 056316.

Xu, L., Zhang, W.W., Nagel, S.R., 2005b. Drop splashing on a dry smooth surface. Phys. Rev. Lett. 94, 184505.
Yarin, A.L., 2006. Drop impact dynamics: Splashing, spreading, receding, bouncing, Annu. Rev. Fluid. Mech. 159-192.

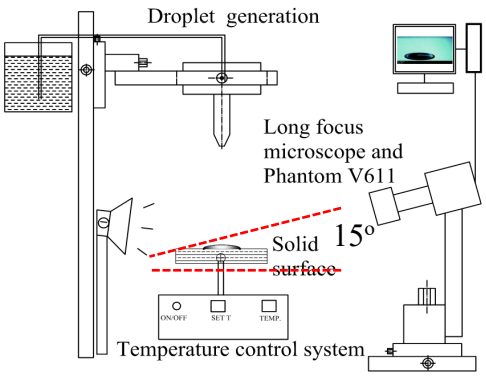

Figure 1 Sketch of the experimental system

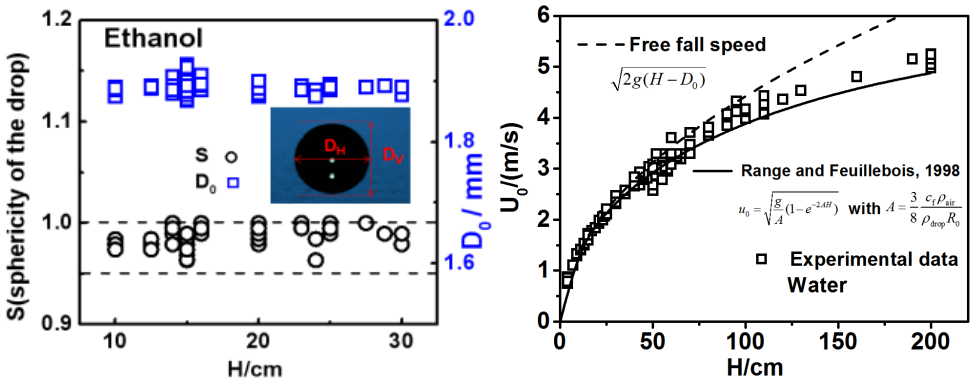

Figure 2 (a) Sphericity and size repeatability of the typical droplets;

(b) droplet velocity before impact, experiments and predictions.

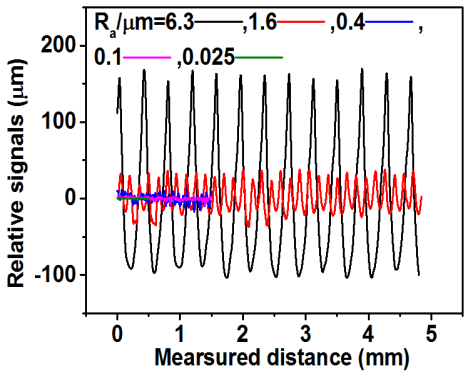

Figure 3 The TR Profile resolved relative surface roughness signals for different standard reference specimens

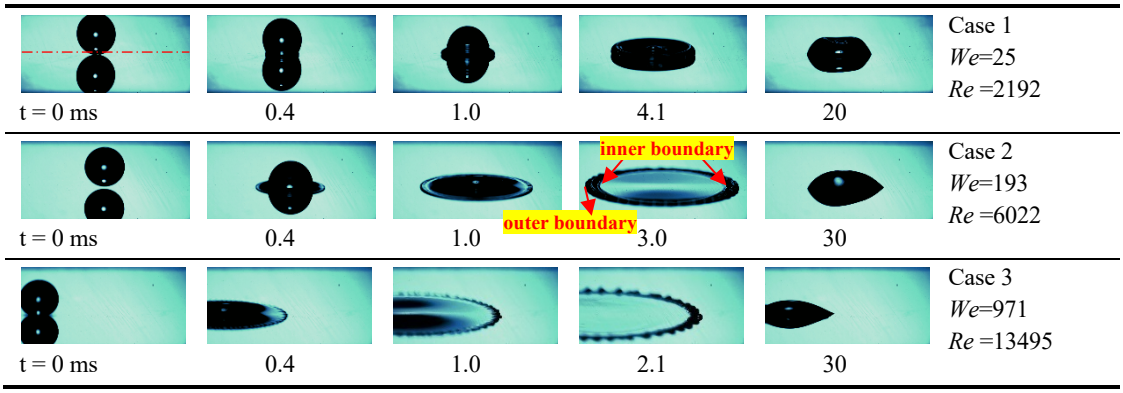

Figure 4 Images of a water droplet impacting on a solid surface for different Weber numbers. R_a = 0.025μm; No splashing is observed.

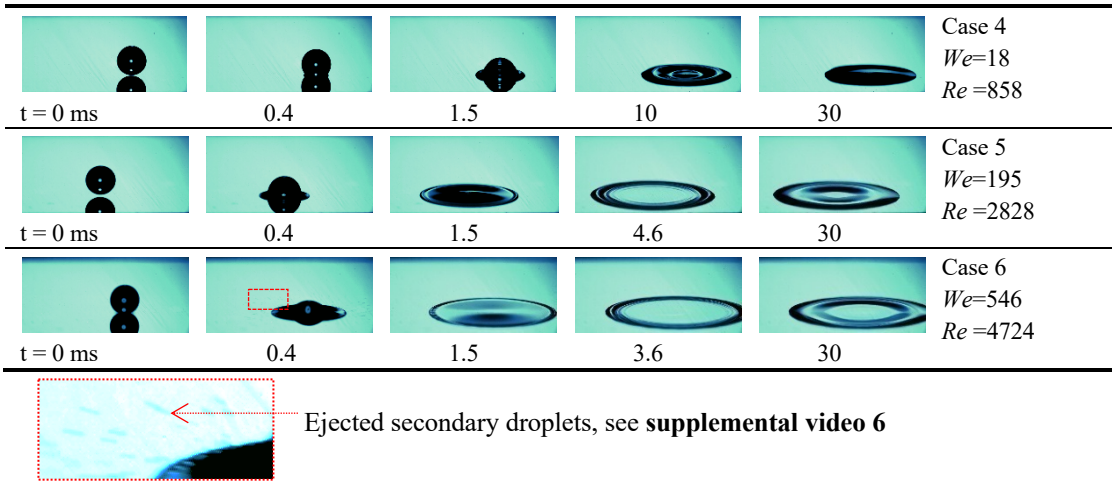

Figure 5 Images of a decane droplet impacting on a solid surface for different Weber numbers. Ra = 0.025μm; splashing is observed for case 6. The supplemental video is more obvious.

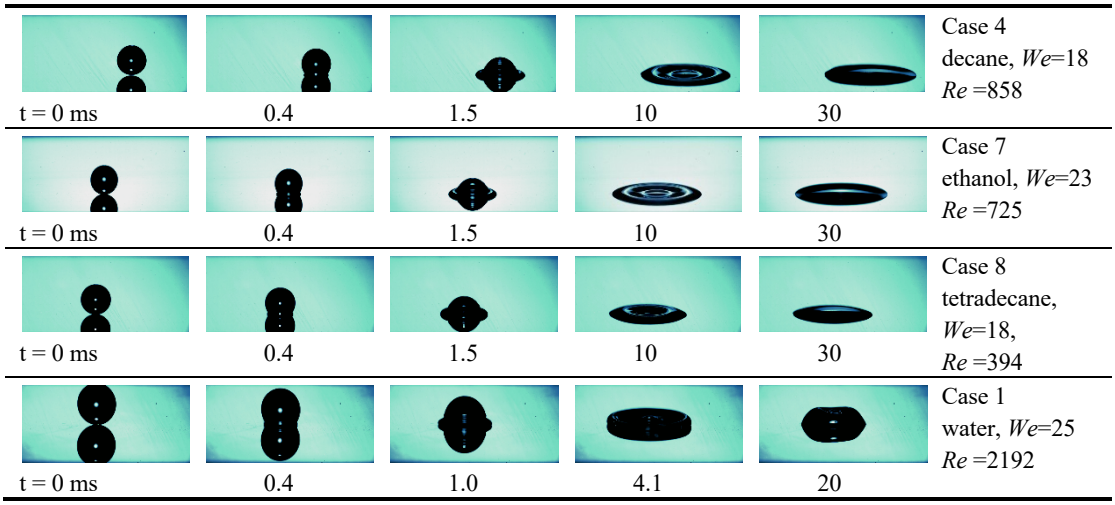

Figure 6 Images of different liquid droplet impacting on a solid surface for $We \approx 20$. R_a = 0.025μm.

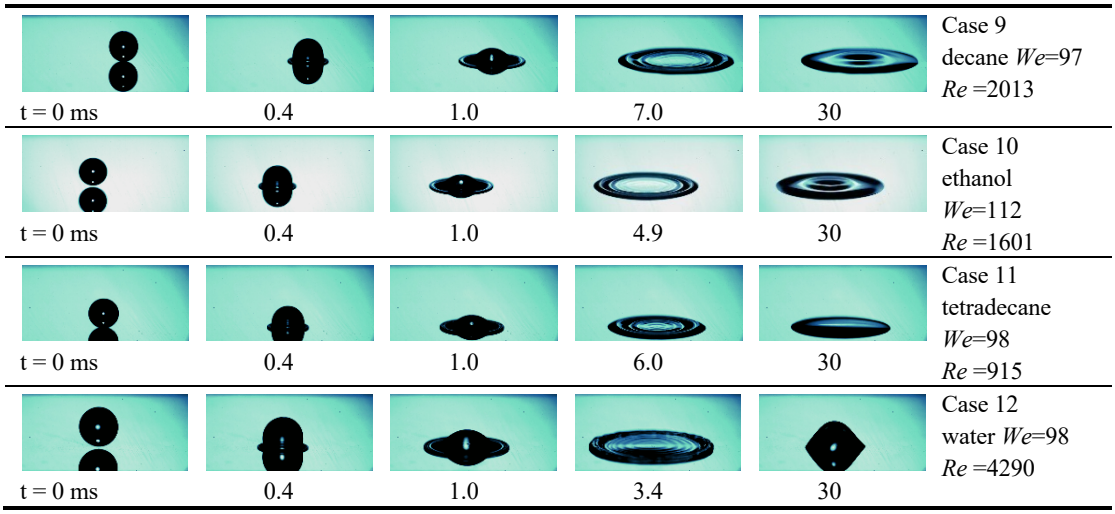

Figure 7 Images of different liquid droplet impacting on a solid surface for $We \approx 100$. $R_a = 0.025$ μm.

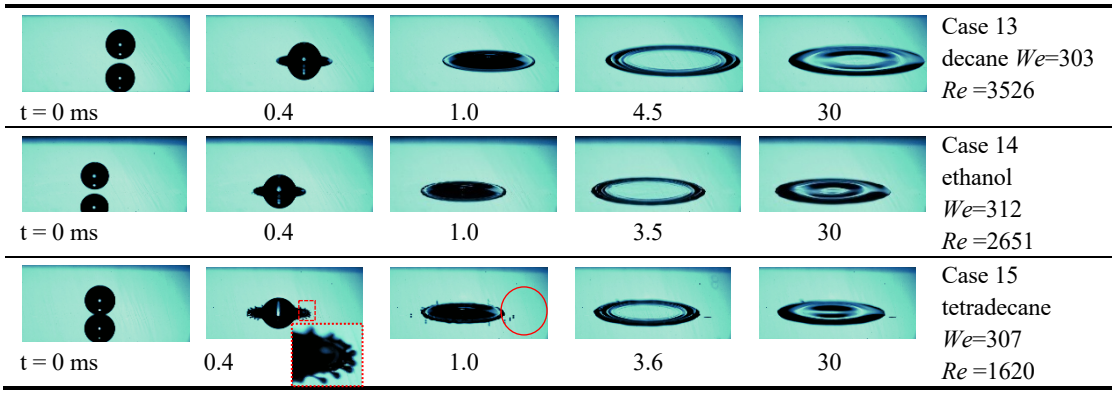

Figure 8 Images of different liquid droplet impacting on a solid surface for $We \approx 300$. $R_a = 0.025$μm. Secondary droplets are observed for tetradecane droplet.

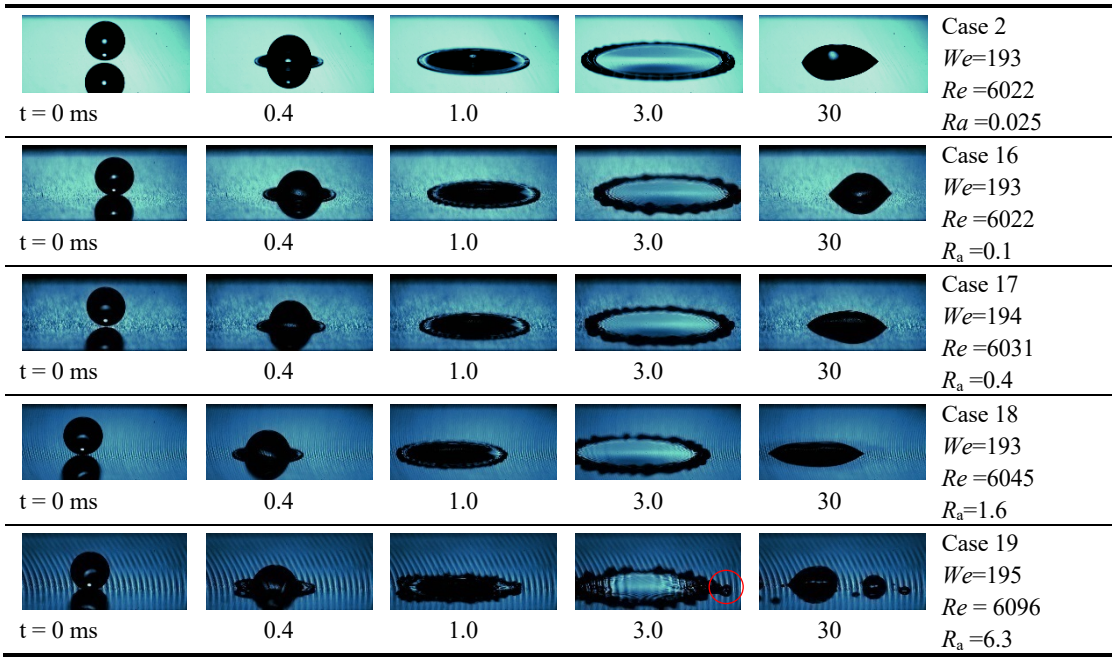

Figure 9 Images of a water droplet impacting on solid surfaces with increased roughness for $We \approx 200$. Secondary droplets are observed for rough surfaces.

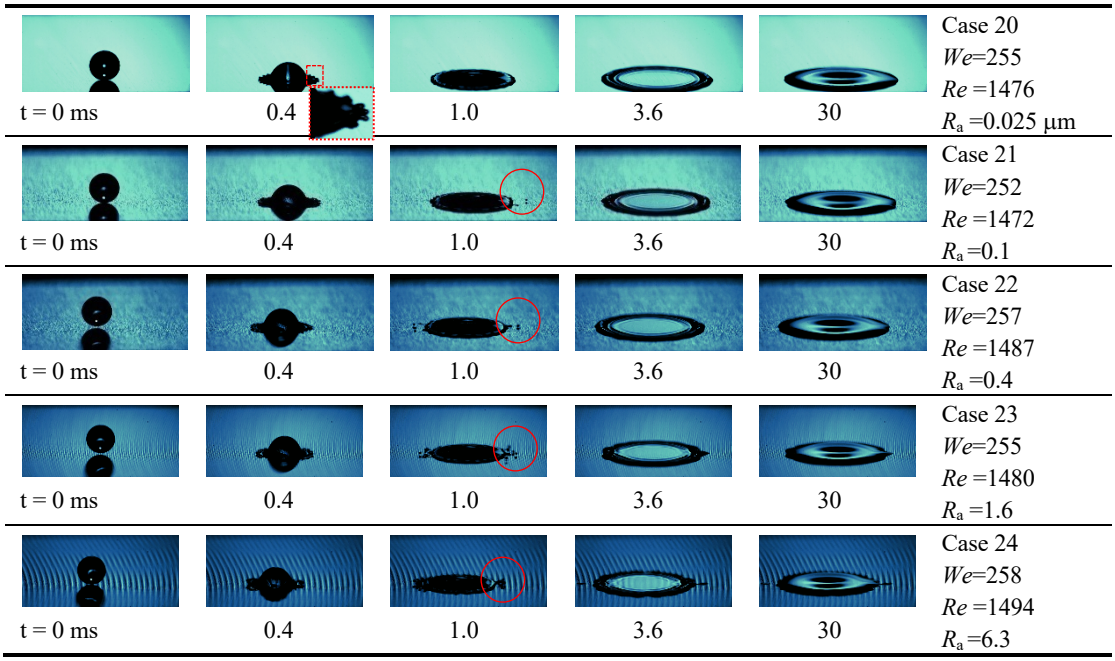

Figure 10 Images of a tetradecane droplet impacting on solid surfaces with increased roughness for $We \approx 250$. Secondary droplets are observed for rough surfaces.

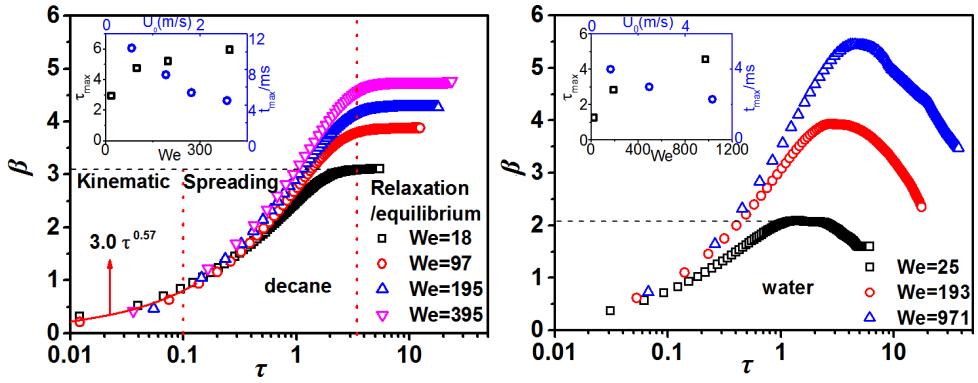

Figure 11 Normalized spreading diameter of droplet impact on a relatively smooth surface (R_a=0.025 μm) as a function of normalized time for different *We*; (a) Decane, (b) water.

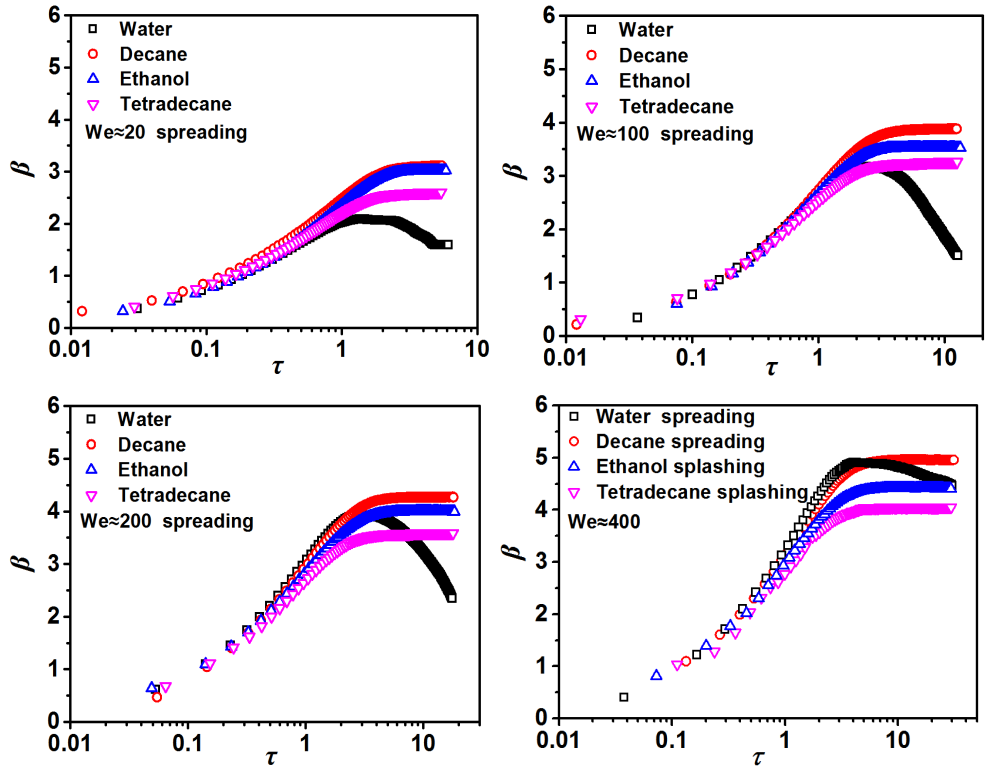

Figure 12 Normalized spreading diameter of droplet impact on a relatively smooth surface (R_a= 0.025 μm) as a function of normalized time for different liquids; (a) $We \approx 20$, (b) $We \approx 100$, (c) $We \approx 200$, (d) $We \approx 400$.

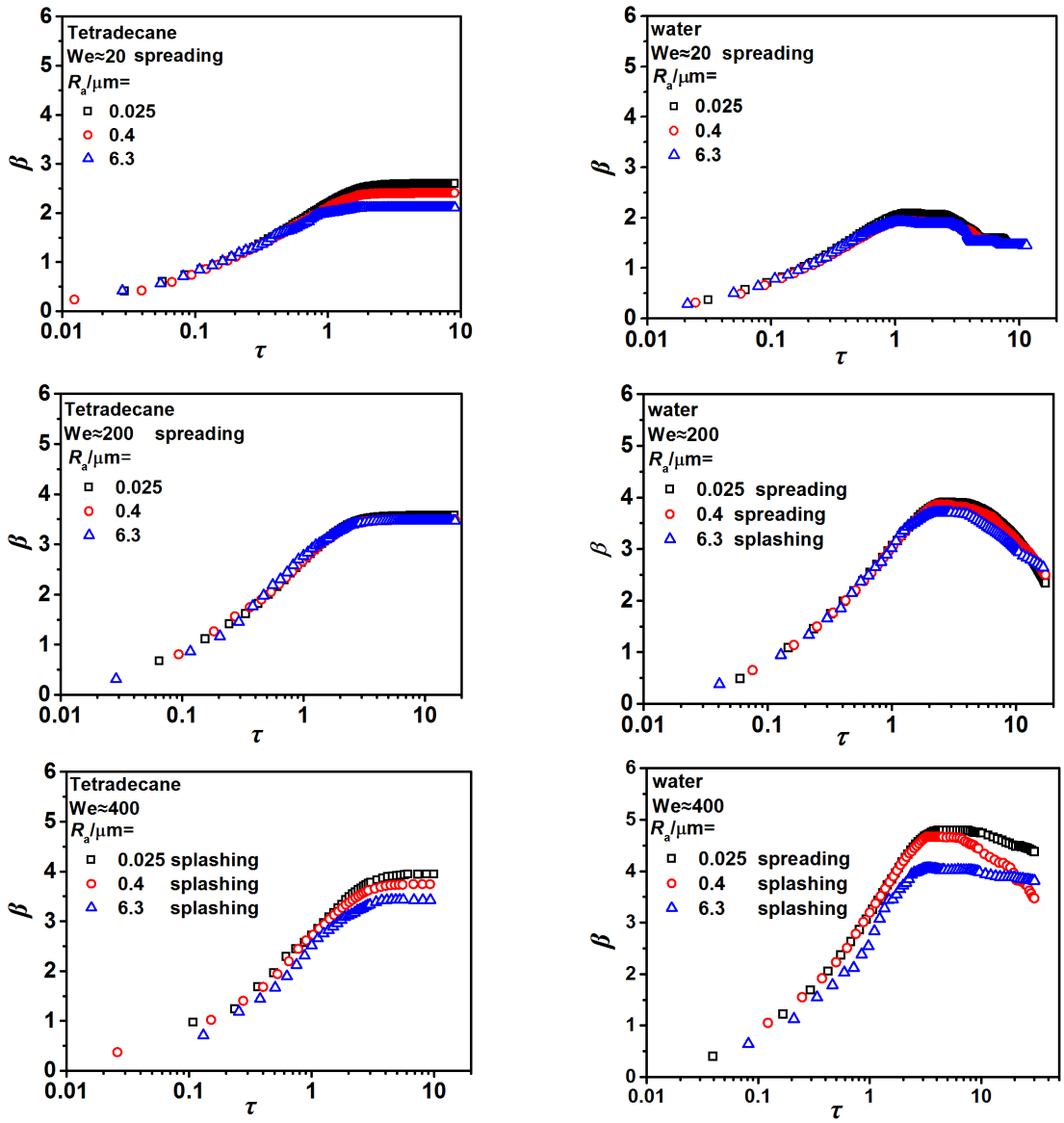

Figure 13 Normalized spreading diameter of droplet impact on a surface with different R_a as a function of normalized time ; (a) Tetradecane, $We \approx 20$, (b) water, $We \approx 20$, (c) tetradecane, $We \approx 200$, (d)water, $We \approx 200$ (e) tetradecane, $We \approx 400$ (f) water, $We \approx 400$

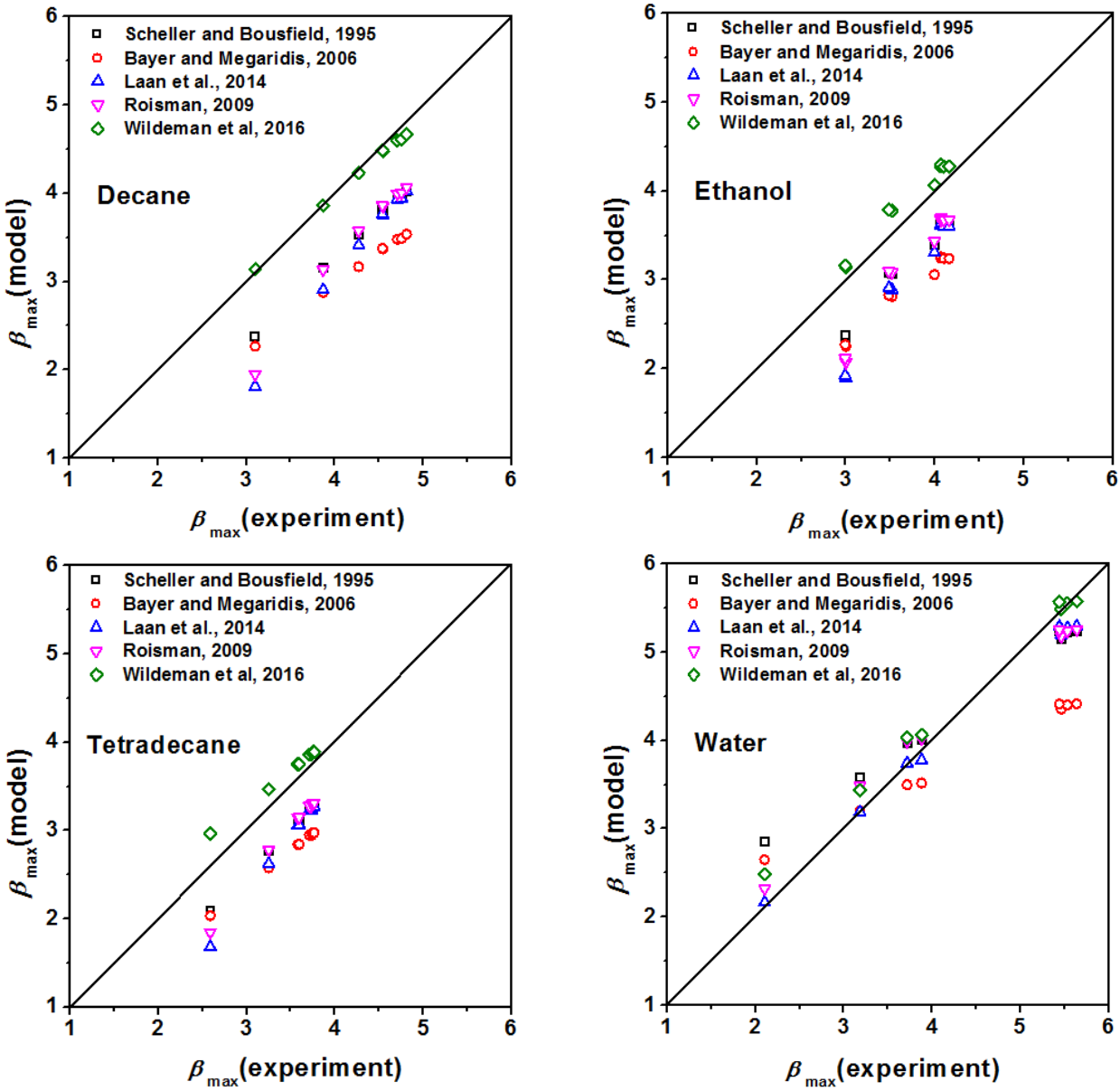

Figure 14 Comparison of several models from Table 2 and the measured β_{max} in this work on smooth surfaces.

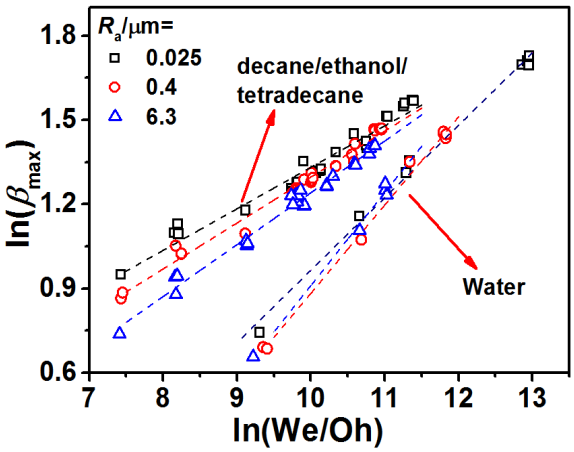

Figure 15 Measured β_{max} as a function of ln(*We*/*Oh*) for surfaces with different R_a.

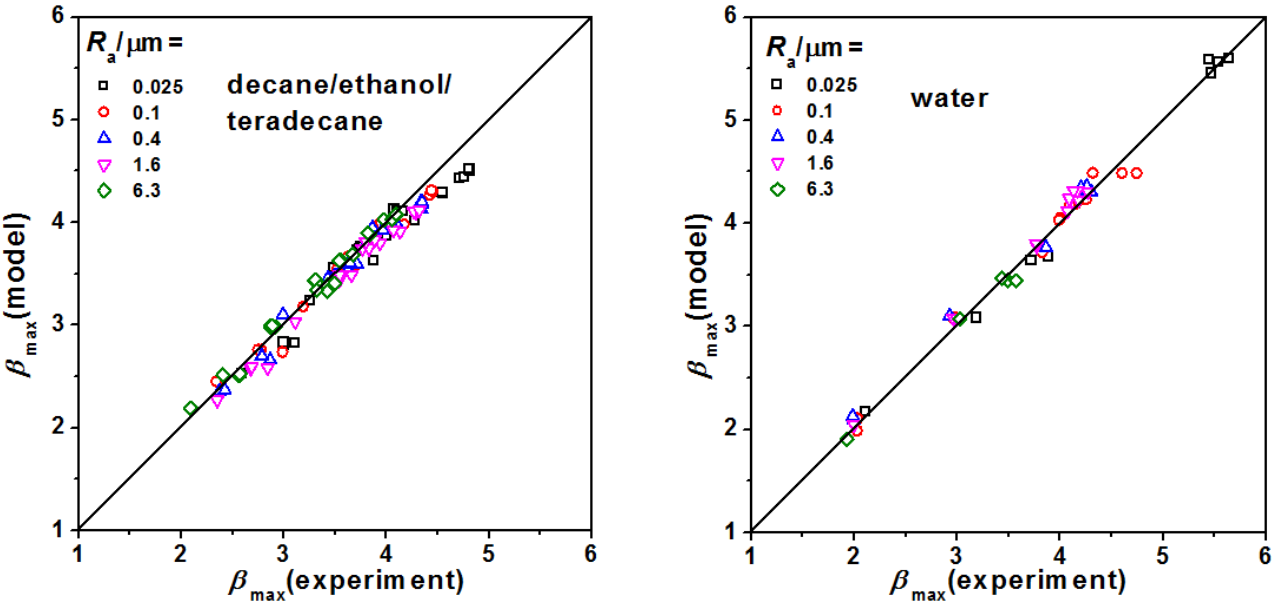

Figure 16 Measured β_{max} in this work and the empirical fitting of Eq. (1).

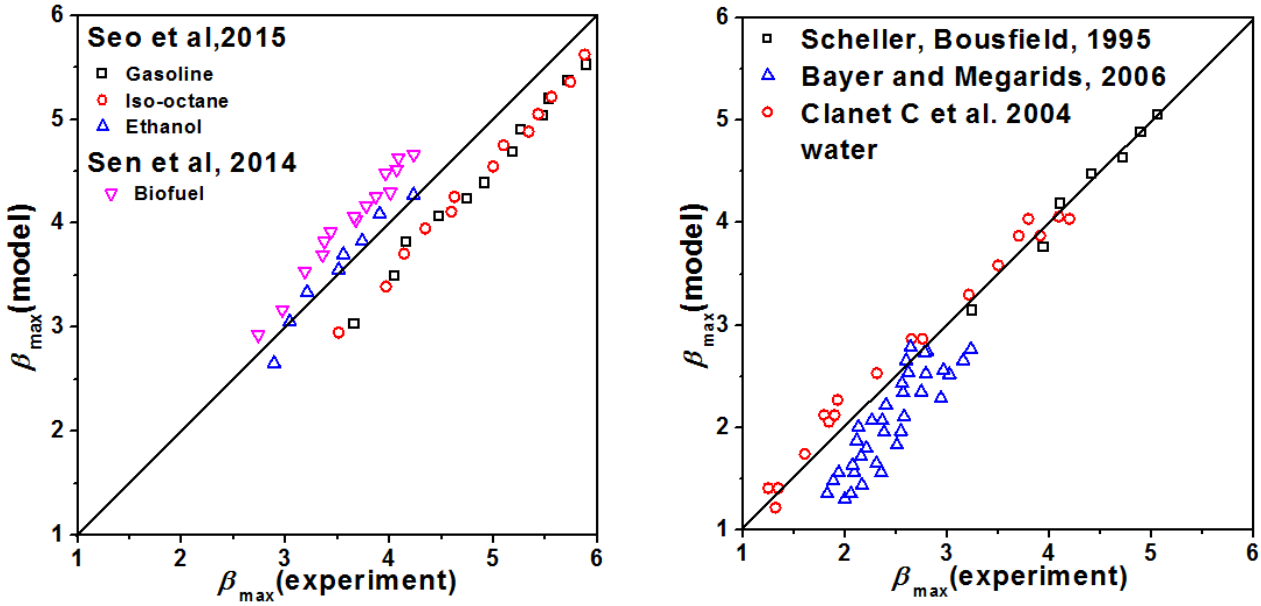

Figure 17 Comparison of the previous measured β_{max} and the empirical fitting of Eq. (1). Experimental data were collected from (Seo et al., 2015), (Sen et al., 2014), (Scheller and Bousfield, 1995), (Clanet et al., 2004), and (Bayer and Megaridis, 2006). We note that all the previous work were done for smooth surfaces.

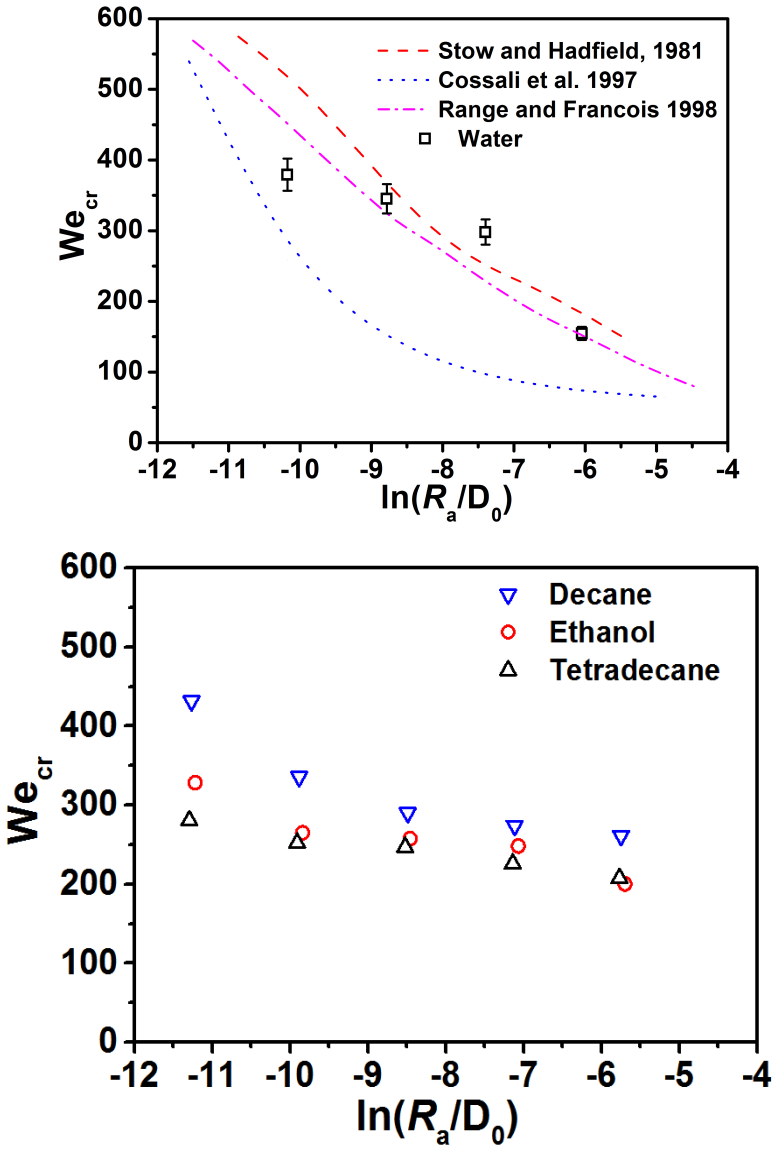

Figure 18 (a) Water droplet impact on different R_a surface, measured We_{cr} vs previous model; The models are for water-aluminium and our data are for water-stainless steel. (b) measured We_{cr} for decane, tetradecane and ethanol data in this work.

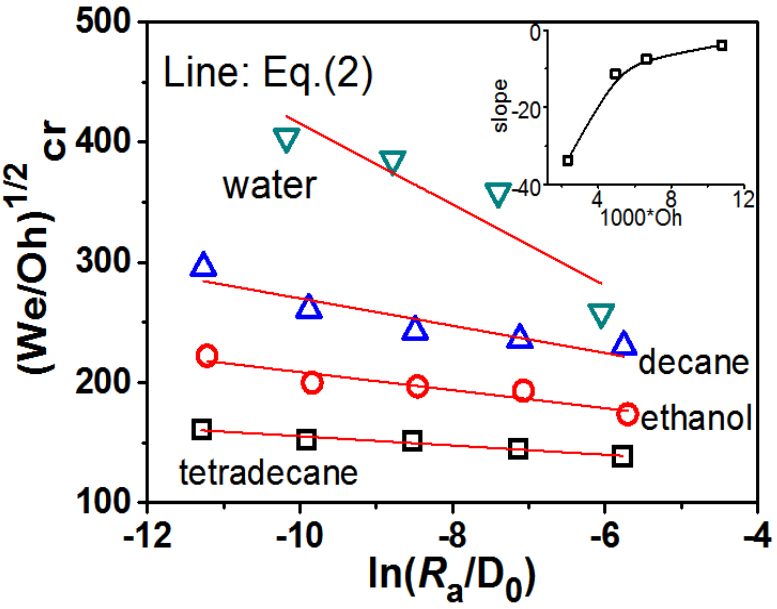

Figure 19 Splashing threshold as a function of R_a. Present measurements and the empirical correlation.

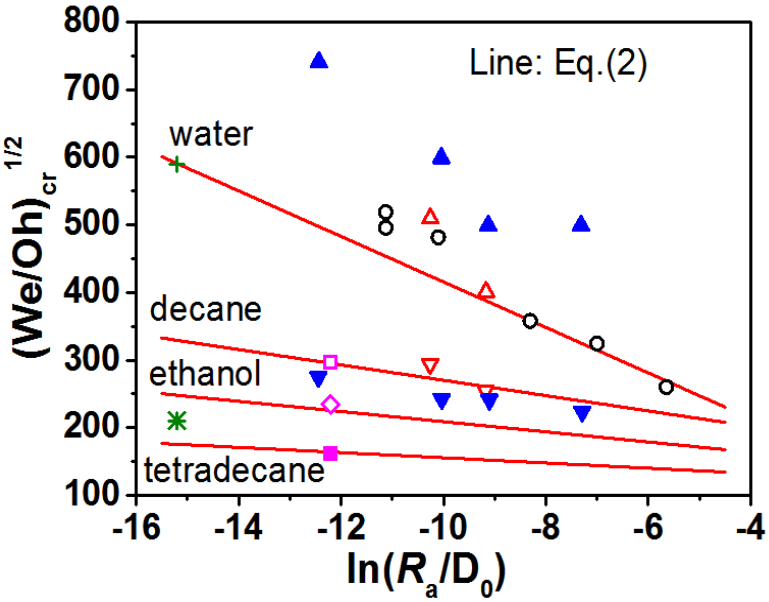

Figure 20 Splashing threshold as a function of R_a. Eq.(2) prediction and the previous experimental data.
(Stow and Hadfield, 1981), ○ water, aluminum & stainless steel plates
(Range and Feuillebois, 1998), △water, aluminum plates ▲water, glass plates▽ethanol, aluminum plates ▼ethanol, glass plates
(Vander Wal et al., 2006a, b),◇ethanol, aluminum plates □decane, aluminum plates ■tetradecane, aluminum plates
(Palacios et al., 2013), + water, glass plate * ethanol, glass plates

Table 1 Physical properties of the tested liquids at 1 atm and 20 °C

Liquid	σ(N·m^{-1})	μ (mPa·s)	ρ (g·cm^3)	D_0	Static contact angle
De-ionized water	0.0720	1.005	0.998	2.64±0.07	50°
Ethanol	0.0223	1.200	0.785	1.89±0.03	7°
Decane	0.0243	0.920	0.730	1.99±0.03	5°
Tetradecane	0.0265	2.18	0.767	2.02±0.03	11°

Table 2 Previous empirical models regarding the maximum spreading diameter

Refs.	Droplet-solid surface	β_{max} equation and brief introduction
(Scheller and Bousfield, 1995)	Glycerin-water-ethanol droplet, smooth polystyrene film/glass	$0.61(We/Oh)^{0.166}$, over predicts β_{max} at low We/Oh,
(PasandidehFard et al., 1996)	Water with surfactants, polished stainless steel surface	$\sqrt{(We+12)/[3(1-\cos\theta_a)+4WeRe^{-0.5}]}$
(Clanet et al., 2004)	Water and mercury droplet, smooth super-hydrophobic surface	$\beta_{max} \sim We^{0.25}$ for $(We/Re^{4/5}) < 1$ $\beta_{max} \sim Re^{0.2}$ for $(We/Re^{4/5}) >= 1$
(Ukiwe and Kwok, 2005)	Water droplet, smooth polymer coated surface	$\beta_{max}^3(3(1-\cos\theta_Y)+4WeRe^{-0.5}) = (We+8)\beta_{max}-8$
(Bayer and Megaridis, 2006)	Water droplet, smooth polished stainless steel surface	$0.72(We/Oh)^{0.14}$, relatively insensitive to surface wettability
(Roisman, 2009)	Water droplet, smooth surface	$Dmax \approx 0.87Re^{1/5} - 0.40Re^{2/5}We^{-1/2}$
(Sen et al., 2014);	Biofuel droplet, smooth stainless steel surface	$\sqrt{(We+12)/[3(1-\cos\theta_a)+4WeRe^{-0.5}]} \sim 1.73We^{0.14}$
(Laan et al., 2014)	Water with/without glycerol, blood droplet, smooth stainless steel surface	$Re^{\frac{1}{5}}P^{\frac{1}{2}}/\left(A+P^{\frac{1}{2}}\right)$, $P = WeRe^{-2/5}$
(Seo et al., 2015)	Gasoline, isooctane, ethanol, smooth aluminum surface	$1.72(We_x/Oh_x)^{0.122}(\mu_{iso}\sigma_{iso}\ \mu_x\sigma_x)$, corrected by the physical properties fluids
(Wildeman et al., 2016)	Water droplet, smooth surface	$\frac{3(1-\cos\theta)}{We}\widetilde{D}_m^2 + \frac{\alpha}{\sqrt{Re}}\widetilde{D}_m^2\sqrt{\widetilde{D}_m-1} = \frac{12}{We}+\frac{1}{2}$ no-slip, We > 30

Table 3 Fitting constants of Eq.s (1) and (2)

Liquids	(a, b) for different R_a in Eq. (1)					c	d
	0.025 μm	0.1 μm	0.4 μm	1.6 μm	6.3 μm	in Eq.(2)	
water	(0.20, 0.26)	(0.15, 0.28)	(0.11, 0.31)	(0.11, 0.31)	(0.09, 0.33)	77.8	-33.7
decane	(0.87,0.15)	(0.75, 0.16)	(0.71, 0.16)	(0.69, 0.17)	(0.55, 0.18)	156.5	-11.4
ethanol	(0.87,0.15)	(0.75, 0.16)	(0.71, 0.16)	(0.69, 0.17)	(0.55, 0.18)	133.6	-7.5
tetradecane	(0.87,0.15)	(0.75, 0.16)	(0.71, 0.16)	(0.69, 0.17)	(0.55, 0.18)	116.8	-3.9

Table 4 Previous empirical models regarding the splashing threshold

Refs.	Droplet, surface combination, roughness range, if specified	Splashing threshold criterion
(Stow and Hadfield, 1981)	Water, with stainless steel and aluminum surface R_a0.05-12	$D_0 U_0^{1.69}$~R_a
(Mundo et al., 1995)	Ethanol, water, water-sucrose-ethanol, with stainless steel surface, R_t=2.8&78μm	K=$OhRe^{1.25}$=57.7
(Cossali et al., 1997)	Data from Refs. (Stow and Hadfield, 1981) and (Mundo et al., 1995)	K=($WeOh^{-0.4}$)= 649+3.76(R_a/D_0)$^{-0.63}$
(Range and Feuillebois, 1998)	Water-glycerol mixtures, and ethanol, with paper, glass, plexiglas, and aluminum surfaces with different roughness	[#]We_{cr}=a log^b(R_0/R_a).

[#] The values of fitting constants a and b depend on their droplet -solid surface combinations.